CONTINUUM DESCRIPTION OF THE TIME- AND STRAIN-DEPENDENT POISSON'S RATIO OF LIGAMENT UNDER FINITE DEFORMATION

by

Aaron Swedberg

A thesis submitted to the faculty of
The University of Utah
in partial fulfillment of the requirements for the degree of

Master of Science

Department of Bioengineering

The University of Utah

May 2014

The University of Utah Graduate School

STATEMENT OF THESIS APPROVAL

The thesis of **Aaron Swedberg**

has been approved by the following supervisory committee members:

Jeffrey A. Weiss	, Chair	**12/10/2013** Date Approved
Heath B. Henninger	, Member	**12/10/2013** Date Approved
Richard D. Rabbitt	, Member	**12/12/2013** Date Approved

and by **Patrick A. Tresco** , Chair/Dean of

the Department/College/School of **Bioengineering**

and by David B. Kieda, Dean of The Graduate School.

ABSTRACT

Ligaments and tendons undergo volume loss when stretched along the primary fiber axis, which is evident by the large, strain-dependent Poisson's ratios measured during quasistatic tensile tests. When continuum constitutive models have been used to describe ligament material behavior they have generally assumed incompressibility, which does not reflect the volume loss seen experimentally. We developed a strain energy equation that can predict both the nonlinear, transversely isotropic behavior as well as the large, strain-dependent Poisson's ratios seen experimentally. This hyperelastic constitutive model was implemented in the finite element solver FEBio and the quasistatic and time-dependent material behaviors were compared to a nearly incompressible constitutive model. The new model was able to predict uniaxial stress-strain behavior comparable to the nearly incompressible model and successfully predicted a large, strain-dependent Poisson's ratio. Biphasic simulations that represented the solid phase with the constitutive model predicted a large outward fluid flux and substantial stress-relaxation, suggesting that the viscoelastic behavior of ligaments and tendons can be predicted by modeling fluid movement when combined with a large Poisson's ratio.

TABLE OF CONTENTS

LIST OF FIGURES

LIST OF SYMBOLS

Symbol	
$\mathbf{F}$	Deformation gradient tensor
$\mathbf{C}$	Right Cauchy-Green deformation tensor
$\mathbf{B}$	Left Cauchy-Green deformation tensor
$\mathbf{a}_0$	Initial fiber direction vector
$\mathbf{a}$	Deformed fiber direction vector
$\mathbf{1}$	3x3 identity tensor
$\mathbf{A}$	General 3x3 tensor
v	Poisson's ratio
λ	Fiber stretch ratio
α	Transverse stretch ratio
W	Strain energy
I_1, I_2, I_3, I_4, I_5	Invariants of the strain energy
J	Jacobian
c_1, c_2	Coefficients in fiber term of the strain energy function
μ	Coefficient in the matrix term of the strain energy function
κ, v_0, m	Parameters of the volumetric strain energy function
σ	Cauchy stress

k_0	Initial permeability
τ	Decay rate coefficient
$\mathbf{S}$	2nd P-K stress
$\boldsymbol{\sigma}$	Cauchy stress
$\mathbb{C}$	Material elasticity tensor
$\mathbb{D}$	Spatial elasticity tensor

ACKNOWLEDGEMENTS

I would like to thank my family and friends for their support and encouragement during my graduate school career. I would like to thank my advisor, Dr. Jeff Weiss, for his insight and guidance in my research and the opportunity to further my education in his lab. I would like to thank my committee members, Dr. Heath Henninger and Dr. Richard Rabbit, for their advice during this process. And finally I would like to thank my fellow MRL lab mates for our fascinating scientific discussions that enriched my higher education and made work enjoyable. Finally, I am grateful for financial support for this research that was provided by the National Institutes of Health Grants #R01AR05334 and #R01GM083925.

CHAPTER 1

INTRODUCTION

Motivation

When fibrous connective tissues such as ligament and tendon are stretched under uniaxial extension along the fiber direction, they exhibit large Poisson's ratios [1-3]. Reported values range from 0.8±0.3 for rat tail tendon fascicles [3] to 2.98±2.59 for bovine flexor tendons [2]. These Poisson's ratios indicate volume loss in the tissue during tensile loading [4]. Since tendons and ligaments are composed of 65-75% water by weight [5], volume loss under tensile loading suggests exudation of fluid from the ligament, as has been reported experimentally [6, 7]. It has been proposed that fluid movement under tensile loading is one of the primary mechanisms by which fibroblasts in the ligament receive and exchange nutrients [8].

Using a micromechanical finite element (FE) model, we demonstrated that the characteristic nonlinear stress-strain behavior and large Poisson's ratios for ligament and tendon can be predicted by modeling a helical orientation within a crimped fiber. Micromechanical models are computationally expensive and thus are not suited for large scale computation, as may be needed for modeling whole joint behavior such as the knee. Continuum models are considerably more computationally economical for FE

simulations, but to date, none have been developed which can describe the large Poisson's ratios seen experimentally. Constitutive models that have been used previously to represent ligaments and tendons in FE simulations generally assume incompressibility [9-12]. For a transversely isotropic material loaded in tension along its fiber direction, this implies a Poisson's ratio of 0.5. This does not accurately reflect experimentally observed ligament and tendon volumetric behavior.

Research Goals

The objective of this research was to develop a continuum based hyperelastic constitutive model that can describe both the stress-strain relationship of tendons and ligaments under tensile loading and the large, strain-dependent Poisson's ratios seen experimentally. This constitutive model was implemented in the open source, nonlinear finite element solver FEBio [13] and combined with a biphasic representation to demonstrate that the time-dependent behavior of ligament during stress relaxation can also be predicted by the model.

Summary of Chapters

Chapter 2 describes the structure and mechanical behavior of ligaments and tendons. Chapter 3 describes the mathematical framework used to derive our ligament constitutive model, the details of the quasistatic simulations, the biphasic simulations and the parameter sensitivity analysis conducted on our model. Results of the simulations are presented in Chapter 4. Chapter 5 provides a discussion of the results of our simulations, how this model improves on previous ligament and tendon constitutive models and the

limitations of our model. Appendices A and B provide a more thorough description of the derivations used to design our constitutive model.

CHAPTER 2

BACKGROUND

Ligament and Tendon Structure, Organization, and Function

Ligaments and tendons are bands of fibrous connective tissue that are critical for proper musculoskeletal function. Ligaments and tendons are extremely similar in structure, and differ primarily in their physiological function. The primary function of ligaments is to connect bone to bone and to guide and restrict joints through their normal range of motion, while tendons connect muscle to bone and transfer muscular forces to the skeleton [14, 15]. The single largest dry weight component of tendons and ligaments is type I collagen (65-80% dry weight), which provides the majority of the tensile strength of the tissue [15]. The rest of the dry weight is composed of an elastin network and proteoglycan components. The behavior of some of these dry weight components have not yet been characterized [14].

The type I collagen in tendons and ligaments is organized into a complex hierarchical structure. On the smallest structural scale, tropocollagen molecules are organized into collagen fibrils. Collagen fibrils are combined into collagen fibers, which then combine to form fascicles, and then finally whole ligaments and tendons (Figure 2.1) [16]. The collagen molecules are formed by elongated fibroblast cells sparsely along the collagen

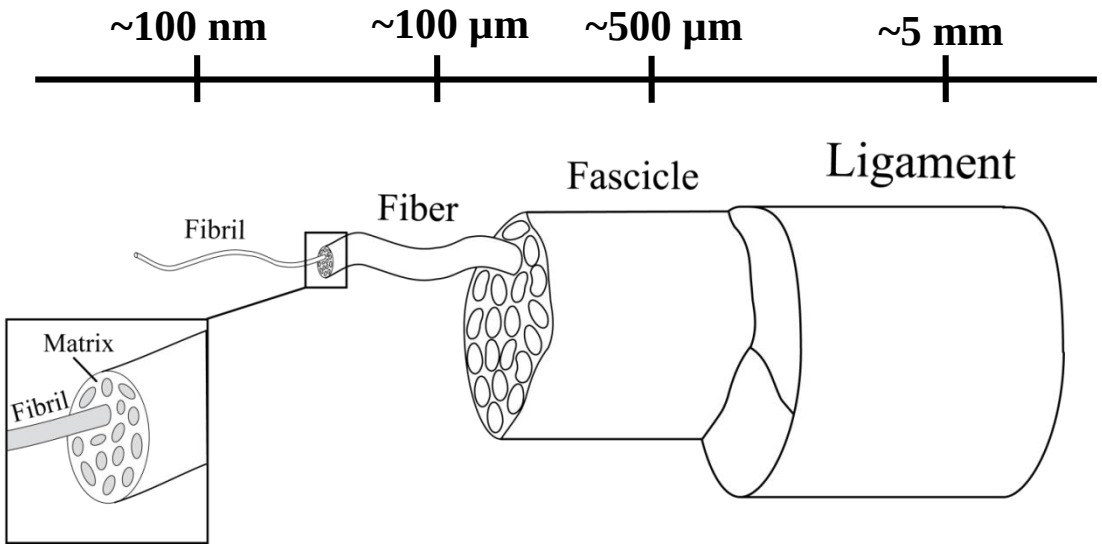

Figure 2.1: Hierarchical structural organization of a ligament. Collagen fibrils at the nanoscale are organized into fibers at the microscale, which are then organized into fascicles and finally whole ligaments.

fibers [17]. Tendons and ligaments are largely avascular [5] and it has been proposed that the fibroblast cells receive nutrients primarily via fluid movement induced by mechanical loading [8].

Mechanical Behavior

The collagen fibers in the ligaments of many articular joints such as the cruciate ligaments of the knee, are oriented primarily along one principle axis, causing transversely isotropic behavior along the primary fiber direction [18]. When loaded along the fiber direction, ligament displays a characteristic nonlinear stress-strain curve (Figure 2.2) [18]. Upon initial loading, the stress-strain curve of ligaments exhibits a "toe region" of low stress response to strain. It is thought that this is due to a crimp like waveform of the collagen fibers straightening out under initial loading, which causes a compliant mechanical response of the tissue [15]. When stretched past the toe region (up to around 6% strain, though the transition point can vary widely between samples [18]), the stress response of ligament becomes linear with increasing applied strain [16]. Ligaments stretched transverse to the fiber direction exhibit much more compliant behavior, suggesting that the mechanical stiffness of the tissues is primarily due to the support of the collagen fibers [18] (Figure 2.2). Ligaments and tendons are composed of up to 75% water by weight which causes time-dependent viscoelastic properties. When loaded with a step displacement, ligaments and tendons exhibit stress relaxation behavior, which causes an initial large peak in the measured stress response of the tissue which dissipates to a smaller equilibrium value [19] (Figure 2.3). Furthermore, when subject to a constant load, ligaments and tendons exhibit creep behavior, where the strain of the

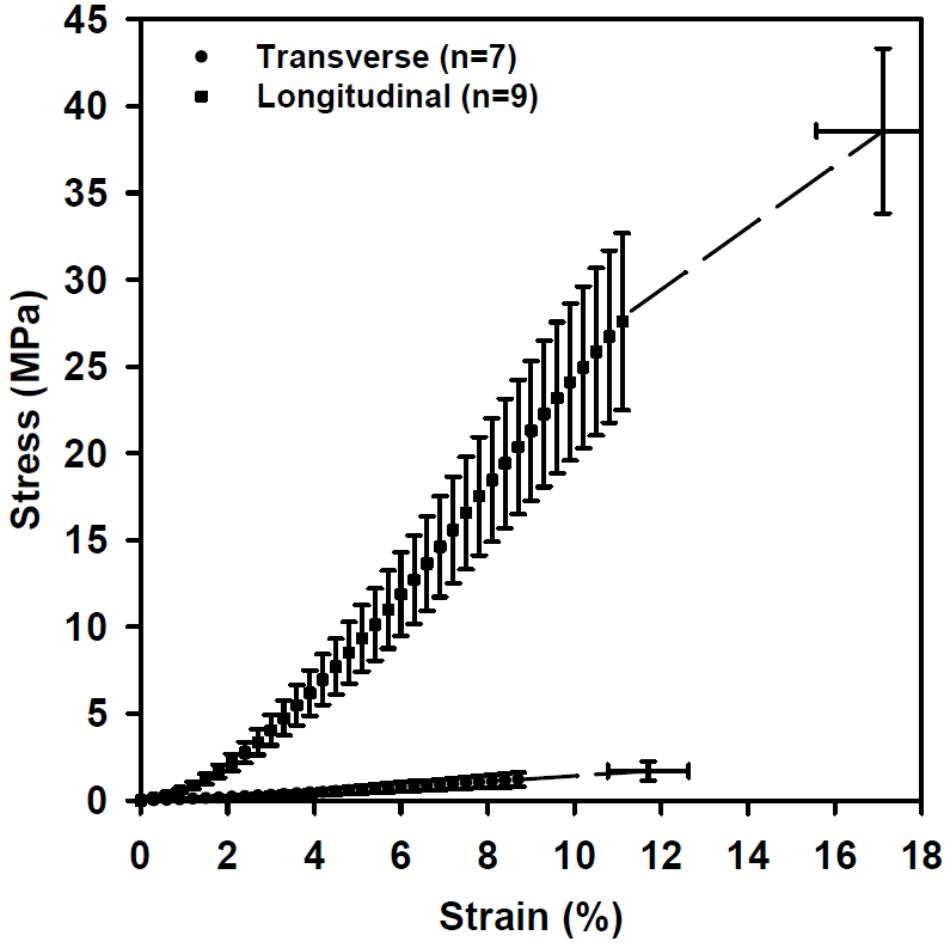

Figure 2.2: Experimentally measured stress-strain behavior of human medial collateral ligament loaded along and transverse to the fiber direction. Reprinted with permission from the American Society of Mechanical Engineers [18].
Quapp, K., and Weiss, J., 1998, "Material characterization of human medial collateral ligament," J Biomech Eng, **120**(6), pp. 757-763.

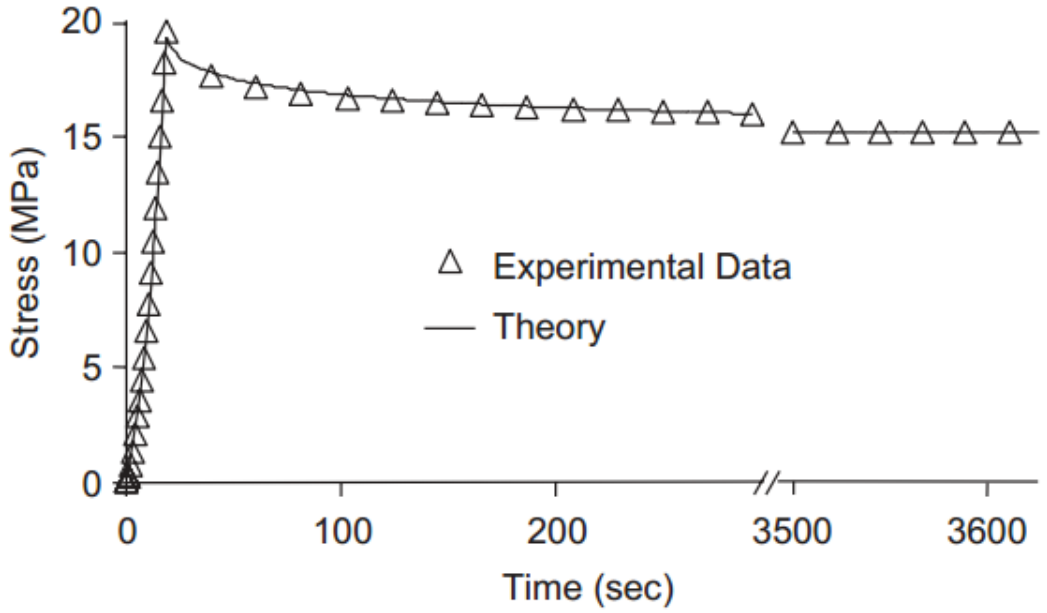

Figure 2.3: Stress relaxation of goat medial collateral ligament with quasilinear viscoelastic curve fit. Reprinted with permission from the American Society of Mechanical Engineers [20].

Abramowitch, S. D., Woo, S. L., Clineff, T. D., and Debski, R. E., 2004, "An evaluation of the quasi-linear viscoelastic properties of the healing medial collateral ligament in a goat model," Ann Biomed Eng, **32**(3), pp. 329-335.

material increases from a smaller value to a larger equilibrium value [16]. Further, when subject to a sinusoidal deformation, the stress response is modulated by amplitude and phase which varies as a function of the loading frequency, providing evidence of load damping [21]. These time- and rate-dependent properties are important for the understanding of joint mechanics under normal or traumatic loading.

Volumetric Behavior

Ligaments and tendons exhibit large Poisson's ratios when loaded along the primary fiber direction, indicating large transverse deformation and volume loss [1-3]. It has been suggested that these large Poisson's ratios are a consequence of the microstructural organization of the tissue, a hypothesis which has been supported by micromechanical models which showed that large Poisson's ratios could be predicted by a helical orientation of the collagen fibrils [4]. It has been experimentally observed that the volume loss implied by the large Poisson's ratios leads to fluid exudation during loading [7, 22]. This fluid movement could play an important role in the transient viscoelastic behavior seen in ligaments and tendons. Furthermore, fluid movement could play a key role in nutrient transport to the fibroblast cells of these tissues [8].

Objectives and Hypotheses

Current continuum constitutive models of tendon and ligament mechanical behavior ignore the large Poisson's ratios seen experimentally and instead assume material incompressibility [9-12]. The goal of our research was to develop a continuum constitutive model for ligament and tendon mechanical behavior that could predict a large

Poisson's ratio by deriving a strain energy equation that constrained the volumetric behavior of the model while producing realistic ligament stress-strain behavior when loaded along the primary fiber direction. We hypothesized that implementing a biphasic representation of our model in the finite element solver FEBio would predict the time-dependent behavior predicted by the simulation when compared to a biphasic implementation of a nearly incompressible model previously used to describe ligament and tendon mechanical behavior.

CHAPTER 3

MATERIALS AND METHODS

Constitutive Model

In order to describe the volumetric behavior of ligament and tendon, we developed a strain energy equation that could describe the volume loss in ligaments due to transverse retraction during uniaxial extension. Consider the uniaxial extension of a transversely isotropic material along the fiber direction with fibers oriented along the *x*-axis. The incremental deformation of the material along the transverse *y* direction, *dy*, will be related to the incremental deformation in the fiber *x* direction, *dx*, via the Poisson's ratio, *v*:

$$\frac{dy}{y} = -v\frac{dx}{x}. \tag{1}$$

If the Poisson's ratio is assumed to be a general function of the deformation in the *x* direction, the integral will take the form:

$$\int_{y_0}^{y_0+\Delta y} \frac{dy}{y} = -\int_{x_0}^{x_0+\Delta x} v(x)\frac{dx}{x}. \tag{2}$$

The variables y_0 and x_0 are the reference lengths in the *y* and *x* directions, respectively, and Δy and Δx are the changes in overall length described by the deformation. The

equation can be expressed in terms of the fiber stretch ratio λ and the transverse stretch ratio α by making the equivalences:

$$y = y_0\alpha, \qquad x = x_0\lambda, \qquad dy = y_0 d\alpha, \qquad dx = x_0 d\lambda. \tag{3}$$

Substituting these values in to Eq. (2), the differential equation can be written as:

$$\int_1^{\alpha^*} \frac{d\alpha}{\alpha} = -\int_1^{\lambda^*} v(\lambda)\frac{d\lambda}{\lambda} \ . \tag{4}$$

The variables λ^* and α^* are actual fiber and transverse stretch ratios. We calculated the Poisson's ratio from previous measurements of fiber and transverse strain in mature rabbit medial collateral ligament (MCL) under uniaxial extension (N=6) [23] (Figure 3.1). Based on these data, we chose to model the Poisson's ratio as a linear function of fiber stretch, λ:

$$v(\lambda) = m(\lambda - 1) + v_0 \, . \tag{5}$$

Here, m and v_0 are the slope and y intercept of the function, respectively. Substituting this expression into Eq. (4) yields the equation:

$$\int_1^{\alpha^*} \frac{d\alpha}{\alpha} = -\int_1^{\lambda^*} (m(\lambda - 1) + v_0)\frac{d\lambda}{\lambda} \ . \tag{6}$$

Integration of both sides of the equation by separation of variables yields an expression for α in terms of the fiber stretch λ and the parameters of our function describing the Poisson's ratio that is valid for finite deformation:

$$\alpha^* = \lambda^{*m - v_0} e^{-m\left(\lambda^* - 1\right)} \ . \tag{7}$$

Since λ^* and α^* are the actual stretch ratios of interest, we drop the asterisks and refer to them as λ and α from hereon. This new definition can be used to derive a strain energy term describing the volumetric deformation of a material. For a representative element of a transversely isotropic material stretched homogeneously along the fiber direction by λ,

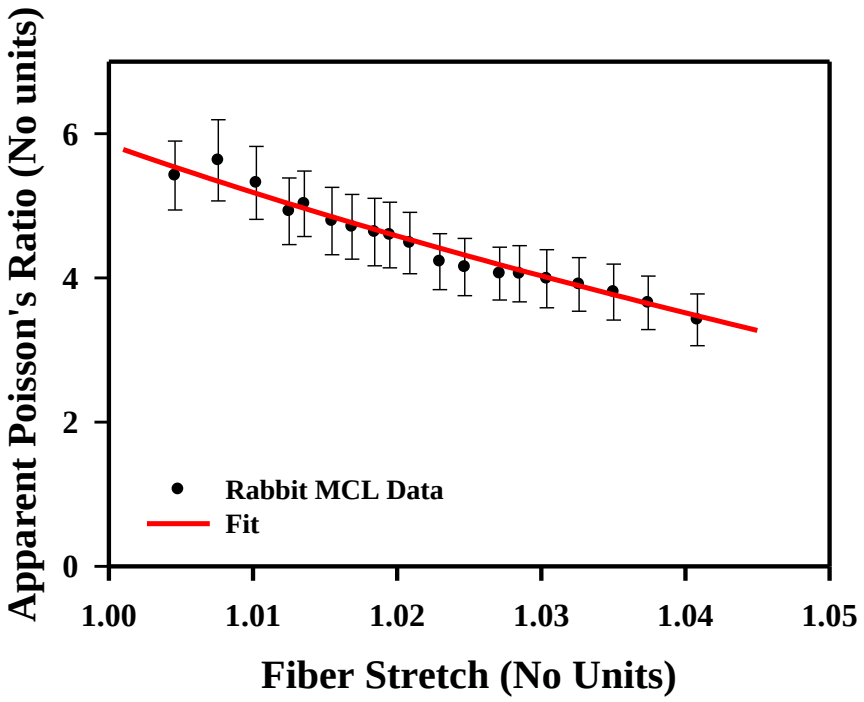

Figure 3.1: The apparent Poisson's ratio as a function of fiber stretch, as calculated from transverse and fiber strains, of mature rabbit medial collateral ligament (N=6). The data were fit to Eq. (14), represented by the red line. The equation fit the data with an R^2 value of 0.967 when the parameters m and v_0 in Eq. (14) were selected to be -100 and 5.85, respectively.

the change in the cross sectional area in the transverse plane is related to the transverse fiber stretch:

$$\frac{da}{dA} = \alpha^2 = \lambda^{2(m-v_0)} e^{-2m(\lambda-1)}. \tag{8}$$

Squaring both sides yields the equation:

$$\left(\frac{da}{dA}\right)^2 = \lambda^{4(m-v_0)} e^{-4m(\lambda-1)}. \tag{9}$$

An alternative equation for the squared area ratio was derived by using Nanson's relation and the Cayley-Hamilton theorem (Appendix A):

$$\left(\frac{da}{dA}\right)^2 = I_5 - I_1 I_4 + I_2 . \tag{10}$$

The variables I_1-I_5 are the strain invariants for a transversely isotropic material:

$$I_1 = \mathrm{tr}(\mathbf{C}), \quad I_2 = \frac{1}{2}\left(\left(\mathrm{tr}(\mathbf{C})\right)^2 - \mathrm{tr}(\mathbf{C}^2)\right), \quad I_4 = \mathbf{a}_0 \cdot \mathbf{C} \cdot \mathbf{a}_0 = \lambda^2, \quad I_5 = \mathbf{a}_0 \cdot \mathbf{C}^2 \cdot \mathbf{a}_0 \ . \tag{11}$$

Here, $\mathbf{C}$ is the right Cauchy-Green deformation tensor, $\mathbf{C} = \mathbf{F}^{\mathbf{T}}\mathbf{F}$ where $\mathbf{F}$ is the deformation gradient tensor, and $\mathbf{a}_0$ is a unit vector defining the initial preferred direction. To our knowledge, the relationship in Eq. (10) has not been presented previously in the literature.

If the deformation of the material is compatible with the deformation prescribed by the parameters of the Poisson's ratio, Eqs. (9) and (10) should be equal to each other and thus their ratio should be equal to 1.0. A strain energy equation was designed to enforce this constraint:

$$W_{vol} = \frac{\kappa}{2}\left(\ln\left(\frac{I_5 - I_1 I_4 + I_2}{I_4^{\,2(m-v_0)} e^{-4m(\lambda-1)}}\right)\right)^2 . \tag{12}$$

Here, κ is a penalty parameter used to enforce the constraint represented by the parameters for the Poisson's ratio. Note that $W_{vol} = 0$ in the reference configuration, is strictly positive and becomes increasingly stiff as κ increases. When combined with an exponential transversely isotropic fiber strain energy representing the behavior of the ligament collagen fibers [18] and a compressible neo-Hookean strain energy equation representing the isotropic behavior of the extrafibrillar matrix [24], the resulting strain energy describes fiber, matrix and volumetric behavior of the tissue:

$$\begin{aligned} W &= W_{fiber} + W_{matrix} + W_{vol}, \\ W_{fiber} &= \frac{1}{2}\frac{c_1}{c_2}\left(e^{c_2(\lambda-1)^2-1}\right), \\ W_{matrix} &= \frac{\mu}{2}(I_1 - 3) - \mu \ln\left(\sqrt{I_3}\right). \end{aligned} \tag{13}$$

The Cauchy stress and spatial elasticity tensors were derived for a general compressible, transversely isotropic hyperelastic material (Appendix B). To our knowledge, these equations have not appeared in the literature previously. These equations were then specialized for the strain energy form in Eq. (13), and the constitutive model was implemented in the nonlinear, open source finite element solver FEBio [13]. The parameters describing the Poisson's ratio, m and v_0 were chosen by fitting the apparent Poisson's ratio, $v_{app} = -\dfrac{\alpha - 1}{\lambda - 1}$, to the experimentally measured Poisson's ratio for the rabbit MCL [23] (Figure 3.1). Note that although the function chosen to describe the Poisson's ratio was a linear equation, as seen in Eq. (5), when transformed by the differential equation in Eq. (6), the apparent Poisson's ratio as predicted by the strain energy equation becomes:

$$v_{apparent} = -\frac{\lambda^{m-v_0} e^{-m(\lambda-1)} - 1}{\lambda - 1} \quad . \tag{14}$$

This equation fit the rabbit MCL data with R^2 = 0.967 when m = -100 and v_0 = 85 (Figure 3.1). The parameters c_1, c_2, and μ were found by fitting the stress-strain behavior along the fiber direction to experimental data for human MCL stretched along the fiber direction [18] (Table 3.1). The initial penalty parameter κ was selected so that the uniaxial Poisson's ratio was within 0.5% of its predicted value as calculated at 3% fiber strain.

Quasistatic Simulation

A single-element uniaxial stress test was used to verify the implementation of the new constitutive model in FEBio. An analytical solution for the Cauchy stress tensor was calculated from the strain energy derivatives using Mathematica (Wolfram Research, Champaign, IL) (Appendix B). The Cauchy stress for uniaxial tension along the fiber direction was calculated using an iterative procedure that determined the transverse stretch α that constrained the transverse stress to zero. In FEBio, prescribed displacements were used to extend the single-element model along the fiber direction to 6% uniaxial strain, and the resulting stress and apparent Poisson's ratio were obtained from the FE calculation. This simulation was repeated with a nearly incompressible constitutive model for ligament behavior, which consisted of a transversely isotropic exponential fiber strain energy term and isotropic Mooney-Rivlin contribution from the matrix [18]. The parameters for the nearly incompressible model were taken from a published study that described the stress response of human MCL loaded along the fiber direction [18].

Table 3.1: Values for the strain energy parameters as listed in Eqs. (12) and (13).

Parameter	Value
c_1 (MPa)	90
c_2	160
μ (MPa)	0.025
K (MPa)	1.55
m	-100
v_0	5.85

Biphasic Simulation

A biphasic simulation was used to assess the ability of the constitutive model to describe the time-dependent material behavior of ligament and tendon. The permeability of the material was based on a strain-dependent isotropic Holmes-Mow constitutive model, fit to published experimental data for the transverse permeability of human MCL [25]. The solid phase was represented by the new constitutive model and was assigned to a quarter symmetry cylindrical mesh with a radius of 1 mm, and the fiber direction was oriented along the long axis of the cylinder (Figure 3.2). The radius of the cylinder was chosen to replicate the approximate cross sectional area of the samples reported in a previous study that examined the viscoelastic material behavior of human MCL [21]. A preliminary stress-relaxation simulation was conducted to select the penalty parameter κ, mimicking the applied displacement protocol of the longitudinal stress relaxation experiment in Bonifasi-Lista et al. [21]. The reaction force curve along the fiber direction, calculated by summing the nodal reaction forces at the location of the applied displacement of the cylinder, was used to quantify the time-dependent behavior of the

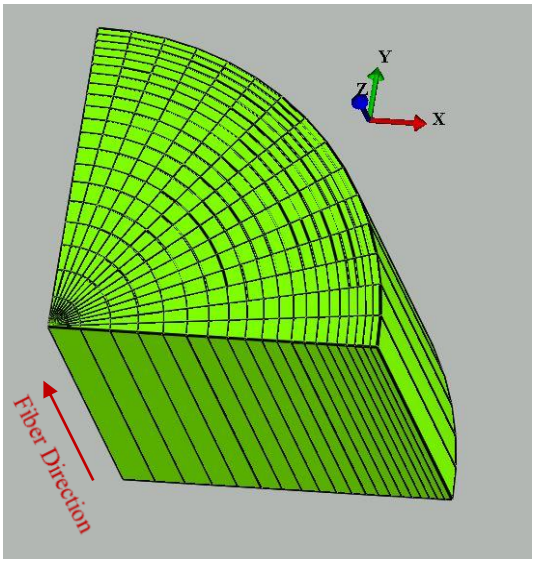

Figure 3.2: Quarter symmetry cylindrical mesh used in the biphasic simulation. The fiber direction was oriented along the long axis of the cylinder as indicated by the red arrow.

model. The penalty parameter κ was altered until the relaxation time constant, τ, defined as the time taken for the reaction force to decrease to 63% of its peak magnitude to the equilibrium magnitude, was approximately 36.1 seconds. This relaxation time was the same as that of the final step of the stress relaxation experiment [21]. This was achieved with a penalty parameter of $\kappa = 1.55$. Since ligaments contain 65-75% water by weight, the fluid volume fraction was selected to be 0.7 [5]. A second stress relaxation simulation was conducted by stretching the model to 3% strain over 1 second. The average fiber stress over all elements, average Poisson's ratio over all elements, and net fluid flux out of the material were plotted as functions of time. This simulation was repeated with the nearly incompressible material description assigned to the solid phase of the model and the time dependent behavior of both models was compared. The mesh density of the cylinder used during this simulation was varied to confirm convergence. A

converged mesh was defined by producing a change in the peak reaction force of less than 0.5% from the previous mesh.

Parameter Sensitivity Study

The penalty parameter κ, matrix coefficient μ, initial permeability k_0, and the radius of the cylinder were increased and decreased by 20% of their initial value used in the biphasic simulation. The sensitivity of the biphasic simulation to the parameters discussed in the previous section was quantified by examining the change in the normalized reaction force at equilibrium of the final displacement step as well as the relaxation time constant, τ.

CHAPTER 4

RESULTS

Quasistatic Simulation

The quasistatic uniaxial simulation revealed that the new model could predict comparable stress-strain behavior to the nearly incompressible model (Figure 4.1A). While the nearly incompressible model predicted a Poisson's ratio that decreased slightly from 0.50 to about 0.48, the new ligament constitutive model predicted a Poisson's ratio that decreased from 5.79 to 2.57 as a function of applied strain (Figure 4.1B).

Biphasic Simulation

The biphasic simulation that used the new model to represent the solid phase predicted substantial stress relaxation. The stress predicted by this simulation peaked at 9.08 MPa and decreased to 4.08 MPa at equilibrium. This equilibrium value was consistent with the stress predicted by the one-element quasistatic simulation at 3% strain (Figure 4.2A). The biphasic simulation that used the nearly incompressible model for the solid phase predicted a constant stress of 4.02 MPa with no relaxation. Simulations that represented the solid phase with the new model also predicted substantial fluid flux out of the material, peaking at 2.37×10^{-2} mm^3/s, while the nearly incompressible simulations

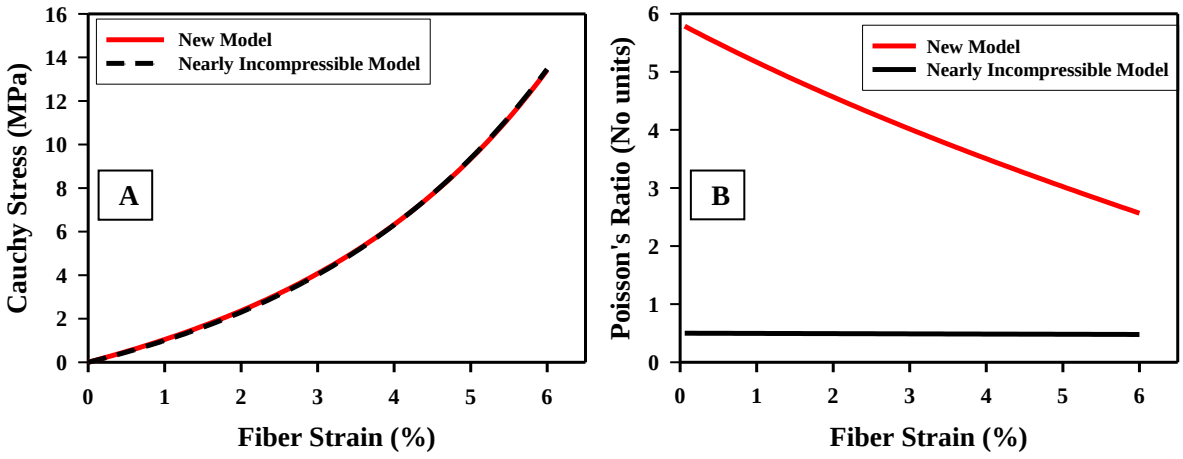

Figure 4.1: Results of the quasistatic simulation. A- The new ligament model was able to predict comparable stress-strain behavior to the previous model. B- The new model predicted an apparent Poisson's ratio that decreased as a function of fiber stretch while the nearly incompressible model predicted a Poisson's ratio of about 0.5 that did not change substantially as a function of fiber strain.

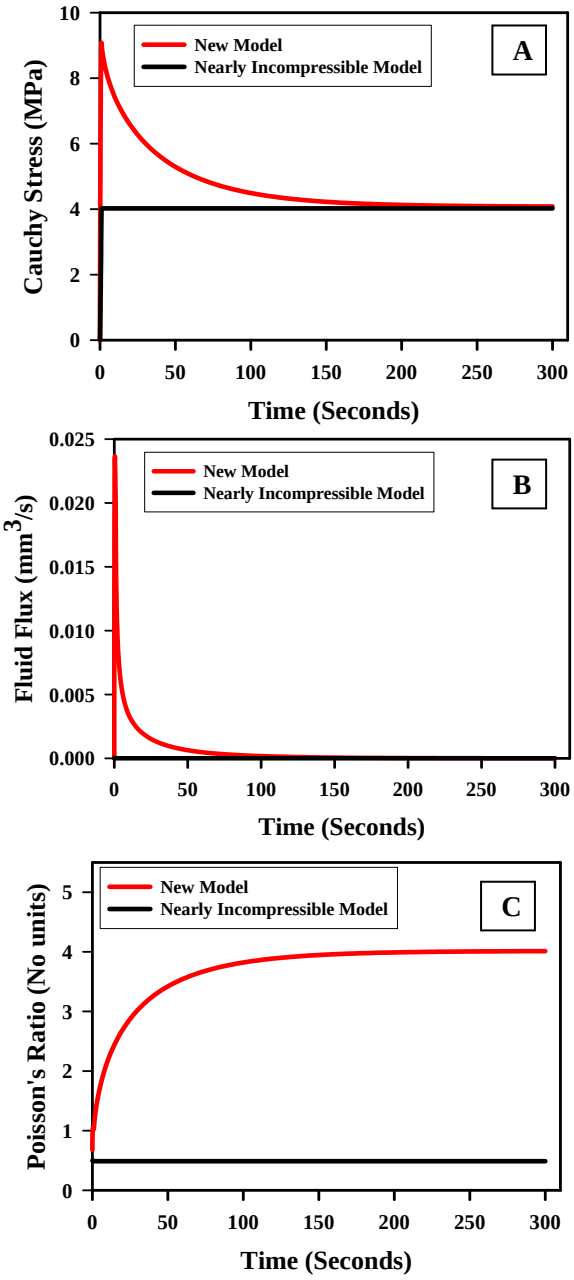

Figure 4.2: Results of the biphasic simulation. A-The Cauchy stress as a function of time during the final displacement step of the biphasic simulation. The new model predicted substantial stress relaxation while the nearly incompressible model did not. B- Net fluid flux out of the outer surface of the cylinder during the final step of the biphasic simulation. The new model predicted a relatively large fluid flux out of the model while the new model predicted nearly no fluid flux. C- The Poisson's ratio of both models during the final step of the biphasic simulation. The Poisson's ratio of the new model increased from a value of near 0.5 to the value predicted by the quasistatic simulation, while the new model predicted a Poisson's ratio of about 0.5.

predicted almost no fluid flux out of the material, peaking at 3.2×10^{-5} mm^3/s upon initial loading (Figure 4.2B). The Poisson's ratio of the nearly incompressible simulations decreased slightly from 0.50 to 0.49, while the Poisson's ratio of the new model increased from 0.68 upon initial loading to 4.01 at full relaxation. This was also the Poisson's ratio predicted by the quasistatic simulation at 3% strain (Figure 4.2C).

Parameter Sensitivity Study

Decreasing the penalty parameter κ by 20% caused the normalized equilibrium reaction force to increase by 13.8% and the relaxation time constant τ to increase by 22.7%, while increasing it by 20% caused the normalized force to decrease by 10.8% and τ to decrease by 11.1%. Decreasing the initial permeability k_0 by 20% caused the normalized equilibrium reaction force to decrease by 0.9% and τ to increase by 24.9%, while increasing it by 20% caused the normalized force to increase by 0.8% and τ to decrease by 15.3%. Altering the matrix parameter μ by 20% in either direction had a negligible effect on both the normalized equilibrium force and relaxation rate. Decreasing the cylindrical radius by 20% caused the normalized equilibrium reaction force to increase by 2.75% and τ to decrease by 33.3%, while increasing it by 20% caused the normalized force to decrease by 1.4% and τ to increase by 40.0% (Figure 4.3).

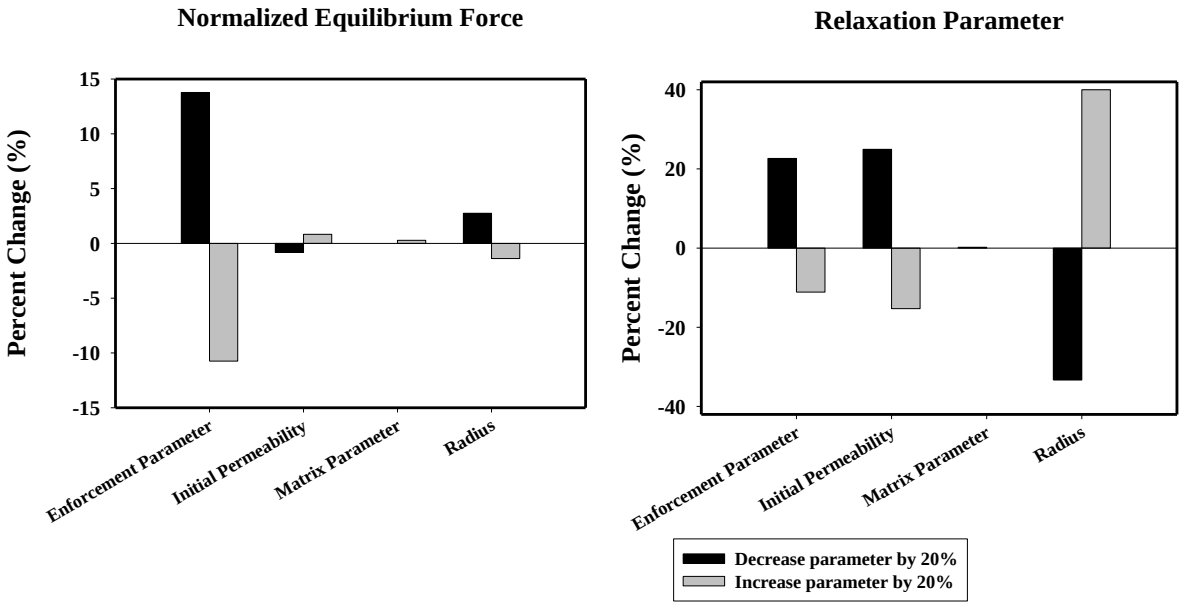

Figure 4.3: Results of the parameter sensitivity study for the biphasic simulation. A- Percent change in the normalized equilibrium reaction force predicted by the biphasic simulation upon increasing and decreasing each parameter by 20%. B- Percent change in the relaxation parameter τ predicted by the biphasic simulation upon increasing and decreasing each parameter by 20%.

CHAPTER 5

DISCUSSION

This research described the development of a volumetric strain energy function that represents the large, strain-dependent Poisson's ratio of ligament and tendon under finite deformation. This equation was combined with expressions describing the strain energy of the collagen fibers and extrafibrillar matrix, resulting in a new constitutive model that was implemented in the finite element solver FEBio. We demonstrated that the new constitutive model can predict the large Poisson's ratios measured experimentally while still predicting a similar uniaxial stress-strain response as a previous nearly incompressible model describing uniaxial tension of human MCL. While previous micromechanical models, have been able to predict a large Poisson's ratio based on microstructural geometry [4], this new model was able to predict this large Poisson's ratio using a penalty based approach which could constrain the Poisson's ratio to a chosen function. This approach was only slightly more computationally expensive than the nearly incompressible continuum models and vastly less expensive than the micromechanical models, which demonstrates its potential for use in large scale, whole joint models. While a linear function was chosen to describe the Poisson's ratio based on existing experimental data of rabbit MCL, the framework outlined in the methods section

shows how any number of functions could be implemented to describe the Poisson's ratio, by substituting the desired equation as a function of λ into Eq. (4) to derive another expression for the squared area ratio, which could then be incorporated into a similar strain energy equation. Thus this method could be used for other applications where it is desirable to constrain the volumetric deformation of a material.

By representing the solid phase of a biphasic material with the new strain energy equation with a realistic solid volume fraction and experimentally based permeability, the model was able to predict time-dependent behavior similar to experimentally observed ligament and tendon viscoelastic behavior. The lateral contraction caused by the enforced large Poisson's ratio had the effect of forcing a substantial amount of fluid out of the material compared to the nearly incompressible model. This is consistent with sources that report fluid exudation from ligaments under uniaxial tension [7, 22]. Furthermore, the pressure buildup caused by the increased fluid pressure also led to an increase in fiber stress which dissipates to the stress value predicted by the quasistatic simulation at equilibrium, resembling the characteristic stress relaxation curve seen in viscoelastic materials. Neither the large fluid flux nor stress relaxation behavior were predicted when the nearly incompressible model was used for the solid phase. The Poisson's ratio of the new model also increased from a small value of 0.68 to the predicted value at 3% strain. The small initial Poisson's ratio suggests that when loading is initiated, the fluid trapped in the material causes nearly incompressible behavior. Then as the fluid is allowed to leave the material, the cylinder contracts, increasing the Poisson's ratio to the predicted value at 3% strain.

Similar behavior has been observed in the measurement of Poisson's ratio during stress relaxation of rat tail tendon fascicles [26]. In the present study, these effects were produced simply by modeling diffusive drag of the fluid components with the solid components, without the inclusion of solid phase viscoelasticity. This conclusion is consistent with those from a previous study by Buckley et al. [27]. During the previous study it was observed that the time dependent lateral contraction of mouse flexor carpi ulnaris tendon was influenced by changes in the ionic concentration of the surrounding fluids. Previous constitutive models that have been used to describe ligament and tendon stress relaxation behavior have explicitly included the time dependent response of the material in their constitutive models [20, 28, 29], and to date, none has attempted to describe the time dependent fluid motion or Poisson's ratio during relaxation.

A parameter sensitivity study was performed to evaluate how the biphasic response of the model was altered by changes in material and biphasic parameters. The equilibrium reaction force was only sensitive to the penalty parameter κ, where increasing κ caused a decrease in the normalized equilibrium reaction force, indicating a larger peak force. This can be explained by understanding that increasing κ caused an increase in the lateral traction force in order to enforce the prescribed volumetric deformation, which in turn caused an increase in fluid pressure leading to a larger peak force. The relaxation time constant τ was sensitive to κ, the initial permeability of the material, and the radius of the model. Again, increasing κ increased the lateral traction force, causing the model to contract more quickly, while increasing the permeability caused the fluid to exit the model more quickly, also allowing a faster relaxation. However, increasing the radius caused the model to relax more slowly, which is again

unsurprising since the fluid can only exude radially outward and increasing the distance that it must cross would increase the diffusive drag of the fluid. This behavior is predicted by biphasic theory and it has been shown during analytical calculations of unconfined compression of cartilage that an increase in radius causes a similar decrease in the relaxation rate. Thus changes in our model parameters were realistic based on our understanding of the behavior of the material.

It is worth noting that κ has two different effects on the mechanical behavior of the model depending on the type of simulation under investigation. For the elastic case, κ behaves as a penalty parameter and serves to enforce the Poisson's ratio. In this case, there is an upper limit of κ that sufficiently enforces the volumetric constraint, and increasing the κ above this value no longer affects the results of the simulation. However, in the biphasic case κ takes on a physical interpretation, in which it determines the lateral traction force that drives the volumetric contraction. Although the final equilibrium value of the Poisson's ratio is the same provided the value of κ is above the upper limit as determined by the elastic case, increasing κ past this value has the added effect of increasing the lateral traction force, causing a faster relaxation rate and larger peak reaction force. Thus for simulations where only the elastic behavior is of interest it is only necessary to select κ to sufficiently enforce the desired Poisson's ratio. For biphasic simulations, however, κ must be determined based on time-dependent experimental data. Methods to decouple these two effects are potential areas for further investigation.

There are several limitations of the present approach that merit discussion. First, the constitutive model was parameterized based solely on experimental measurements of

uniaxial stress-strain behavior and Poisson's ratio. This was a reasonable approach given the goals of the analyses. Second, the matrix was modeled using a compressible neo-Hookean strain energy, which leads to a linear stress-strain relationship in shear or transverse to the fiber direction. The experimentally measured force response of ligament under shear loading along the fiber direction is more accurately described by an exponential function [30]. Since transverse loading was not the focus of the study, this was an appropriate simplification. A final limitation is that the data used to parameterize the Poisson's behavior of our model was taken from a relatively small range of longitudinal strain, primarily in the toe region of the ligament, and the data used were distinct from the data used to parameterize the stress-strain behavior of our model. Since there is limited data in the literature reporting the Poisson's ratio as a function of fiber stretch, especially at larger values, further experiments must be performed to obtain this data to ensure the model is valid for larger values of strain.

In single-element FE simulations of uniaxial extension at larger fiber strains, we observed that the volume ratio of the element began to increase after λ=1.05. Since the volume ratio under uniaxial tension is $J=\lambda\alpha^2$, we can use Eq. (7) for α as a function of λ to obtain an analytical expression for the volume ratio as a function of fiber stretch. This equation has a minimum at $\lambda = \frac{1+2m-2v_0}{2m}$, which for the parameters listed in Table 1, occurs at λ =1.053. The volume ratio is predicted to increase after this stretch ratio, as we observed. Although the increase in volume at higher values of fiber stretch does not reflect realistic volumetric behavior, it is a mathematical consequence of using a linear function to describe the Poisson's ratio. This observation emphasizes the need for experimental studies of the Poisson's ratio at higher values of axial strain, to guide the

specification of a function that more accurately reflects realistic ligament volumetric behavior over the entire physiological range of axial strain.

APPENDIX A

CROSS SECTIONAL AREA DERIVATION USING THE CAYLEY-HAMILTON THEOREM AND NANSON'S RELATION

Using Nanson's relation [31] and the Cayley-Hamilton equation [32], we can derive an alternate form of $\left(\frac{da}{dA}\right)^2$ as represented by equation (9) in terms of the transversely isotropic strain invariants as shown below:

$$\begin{aligned} I_1 &= \mathrm{tr}(\mathbf{C}) \\ I_2 &= \frac{1}{2}\left(\left(\mathrm{tr}(\mathbf{C})\right)^2 - \mathrm{tr}(\mathbf{C}^2)\right) \\ I_3 &= \det(\mathbf{C}) = J^2 \\ I_4 &= \mathbf{a}_0 \cdot \mathbf{C} \cdot \mathbf{a}_0 = \lambda^2 \\ I_5 &= \mathbf{a}_0 \cdot \mathbf{C}^2 \cdot \mathbf{a}_0 \end{aligned} \quad , \tag{15}$$

The tensor **C** is the right Cauchy-Green deformation tensor, $\mathbf{C}=\mathbf{F}^T\mathbf{F}$, where **F** is the deformation gradient and $J = \det(\boldsymbol{F})$ is the volume ratio. The variable λ is the stretch ratio along the direction of loading, **a** and $\mathbf{a}_0$ are the deformed and reference fiber direction unit vectors, respectively, and *da* and *dA* are the deformed and undeformed material cross sectional areas, respectively, normal to the direction of loading. Nanson's relation states that for a given area:

$$\mathbf{a}\,da = J\mathbf{F}^{-T} \cdot \mathbf{a}_0\,dA \ . \tag{16}$$

The Cayley-Hamilton theorem states that for any tensor **A**:

$$\mathbf{A}^3 - I_1\mathbf{A}^2 + I_2\mathbf{A} - I_3\mathbf{1} = \mathbf{0} \ . \tag{17}$$

By selecting the right Cauchy-Green deformation tensor $\mathbf{C}=\mathbf{F}^T\mathbf{F}$ to replace the **A** tensor in (17), we are left with:

$$\mathbf{C}^3 - I_1\mathbf{C}^2 + I_2\mathbf{C} - I_3\mathbf{1} = \mathbf{0} \ . \tag{18}$$

Rearranging equation (18) and noting that $I_3 = J^2$:

$$\mathbf{C}^3 - I_1\mathbf{C}^2 + I_2\mathbf{C} = J^2\mathbf{1} \ . \tag{19}$$

Multiplying (16) with $J\mathbf{F}^T$:

$$J\mathbf{F}^T \cdot \mathbf{a}da = (J^2\mathbf{1}) \cdot \mathbf{a}_0 dA \ . \tag{20}$$

By substituting (19) into the right hand side of (20), we obtain:

$$J\mathbf{F}^T \cdot \mathbf{a}da = (\mathbf{C}^3 - I_1\mathbf{C}^2 + I_2\mathbf{C}) \cdot \mathbf{a}_0 dA \ . \tag{21}$$

The initial fiber direction $\mathbf{a}_0$ transforms into the current configuration using the deformation gradient:

$$\mathbf{F} \cdot \mathbf{a}_0 = \lambda\mathbf{a} \ , \tag{22}$$

which can be rearranged to show that $\mathbf{a} = \frac{1}{\lambda}\mathbf{F}\mathbf{a}_0$. We can thus replace **a** in (21) to show that:

$$\frac{J}{\lambda}\mathbf{F}^T\mathbf{F} \cdot \mathbf{a}da = (\mathbf{C}^3 - I_1\mathbf{C}^2 + I_2\mathbf{C}) \cdot \mathbf{a}_0 dA \ , \tag{23}$$

which can also be written as:

$$\frac{J}{\lambda}\mathbf{C} \cdot \mathbf{a}_0 da = (\mathbf{C}^3 - I_1\mathbf{C}^2 + I_2\mathbf{C}) \cdot \mathbf{a}_0 dA \ . \tag{24}$$

Premultiplying (24) by $\mathbf{a}_0 \cdot \mathbf{C}^{-1}$ gives

$$\frac{J}{\lambda}\mathbf{a}_0 \cdot \mathbf{C}^{-1}\mathbf{C} \cdot \mathbf{a}_0 da = \mathbf{a}_0 \cdot \mathbf{C}^{-1}(\mathbf{C}^3 - I_1\mathbf{C}^2 + I_2\mathbf{C}) \cdot \mathbf{a}_0 dA \ , \tag{25}$$

which can also be written as:

$$\frac{J}{\lambda} da = (\mathbf{a}_0 \cdot \mathbf{C}^2 \cdot \mathbf{a}_0 - I_1\mathbf{a}_0 \cdot \mathbf{C} \cdot \mathbf{a}_0 + I_2\mathbf{a}_0 \cdot \mathbf{a}_0) dA \ . \tag{26}$$

We can simplify the terms on the right hand side into strain invariants based in (15) and divide both sides by *dA*:

$$\frac{J}{\lambda}\frac{da}{dA} = I_5 - I_1 I_4 + I_2 \ . \tag{27}$$

Since, for a deformation of a cube of transversely isotropic material along the fiber direction the volume ratio of the deformation will be given by:

$$J = \lambda\alpha^2 \ , \tag{28}$$

where α is the stretch ratio in the directions transverse to the direction of loading. For a representative cube of material, the change in cross sectional area transverse to the fiber direction are related by:

$$\alpha^2 = \frac{da}{dA} \ . \tag{29}$$

Thus by rearranging (28), replacing $\frac{J}{\lambda}$ in (27):

$$\left(\frac{da}{dA}\right)^2 = I_5 - I_1 I_4 + I_2 \ . \tag{30}$$

APPENDIX B

CAUCHY STRESS AND SPATIAL ELASTICITY TENSOR DERIVATION FOR A TRANSVERSELY ISOTROPIC COMPRESSIBLE HYPERELASTIC MATERIAL

In order to implement the strain energy equation presented in this paper in the finite element solver FEBio, the Cauchy stress tensor and spatial elasticity tensor must be calculated. The derivation of a general form for of both the Cauchy stress tensor and spatial elasticity tensors for a transversely isotropic compressible hyperelastic material is presented in this appendix.

For some strain energy equation W, the 2nd P-K stress $\mathbf{S}$ can be derived using the right Cauchy-Green deformation tensor $\mathbf{C}$:

$$\mathbf{S} = 2\frac{\partial W}{\partial \mathbf{C}} \ . \tag{31}$$

If W is expressed in terms of the transversely isotropic strain invariants I_α, where α ranges from 1 to 5 as shown in (15), using the chain rule, equation (31) can be expressed as:

$$\mathbf{S} = 2\sum_{\alpha=1}^{5}\left(\frac{\partial W}{\partial I_\alpha}\frac{\partial I_\alpha}{\partial \mathbf{C}}\right) . \tag{32}$$

The derivatives $\frac{\partial I_\alpha}{\partial \mathbf{C}}$ for each of the transversely isotropic strain invariants are as follows:

$$\begin{aligned}
\frac{\partial I_1}{\partial \mathbf{C}} &= \mathbf{1} \\
\frac{\partial I_2}{\partial \mathbf{C}} &= I_1\mathbf{1} - \mathbf{C} \\
\frac{\partial I_3}{\partial \mathbf{C}} &= I_2\mathbf{1} - I_1\mathbf{C} + \mathbf{C}^2 = I_3\mathbf{C}^{-1} \quad . \\
\frac{\partial I_4}{\partial \mathbf{C}} &= \mathbf{a}_0 \otimes \mathbf{a}_0 \\
\frac{\partial I_5}{\partial \mathbf{C}} &= \mathbf{a}_0 \otimes \mathbf{C}\cdot\mathbf{a}_0 + \mathbf{a}_0 \cdot \mathbf{C} \otimes \mathbf{a}_0
\end{aligned} \tag{33}$$

The derivatives $\frac{\partial W}{\partial I_\alpha}$ are found based on the specific strain energy equation represented in terms of the invariants, and are henceforth represented as W_α. The 2nd P-K stress can thus be found to be:

$$\mathbf{S} = W_1\mathbf{1} + W_2(I_1\mathbf{1} - \mathbf{C}) + W_3(I_3\mathbf{C}^{-1}) + W_4(\mathbf{a}_0 \otimes \mathbf{a}_0) + W_5(\mathbf{a}_0 \otimes \mathbf{C}\cdot\mathbf{a}_0 + \mathbf{a}_0 \cdot \mathbf{C} \otimes \mathbf{a}_0) \quad . \tag{34}$$

The Cauchy stress can be found by transforming **S** into the current spatial configuration via a push forward operation:

$$\sigma = \varphi * \mathbf{S} \ , \tag{35}$$

where $\varphi *$ represents the push forward operator, which for of some second order tensor **A** is:

$$\varphi * \mathbf{A} = \frac{1}{J}\mathbf{F}\mathbf{A}\mathbf{F}^T \quad . \tag{36}$$

Only the tensors in (34) are transformed by the push forward operation, while the invariants and the strain energy derivatives are constants and can thus be factored out of the transformation. The transformed tensors are as follows:

$$
\begin{aligned}
&\varphi^*\mathbf{1} = \frac{1}{J}\mathbf{F}\mathbf{1}\mathbf{F}^T = \frac{1}{J}\mathbf{B} \\
&\varphi^*\mathbf{C} = \frac{1}{J}\mathbf{F}(\mathbf{F}^T\mathbf{F})\mathbf{F}^T = \frac{1}{J}\mathbf{B}^2 \\
&\varphi^*\mathbf{C}^{-1} = \frac{1}{J}\mathbf{F}(\mathbf{F}^T\mathbf{F})^{-1}\mathbf{F}^T = \frac{1}{J}\mathbf{F}(\mathbf{F}^{-1}\mathbf{F}^{-T})\mathbf{F}^T = \frac{1}{J}\mathbf{1} \\
&\varphi^*(\mathbf{a}_0 \otimes \mathbf{a}_0) = \frac{\lambda^2}{J}(\mathbf{a}\otimes\mathbf{a}) = \frac{I_4}{J}(\mathbf{a}\otimes\mathbf{a}) \\
&\varphi^*(\mathbf{a}_0 \otimes \mathbf{C}\cdot\mathbf{a}_0) = \frac{I_4}{J}(\mathbf{a}\otimes\mathbf{a})\cdot\mathbf{B} \\
&\varphi^*(\mathbf{a}_0 \cdot \mathbf{C}\otimes\mathbf{a}_0) = \frac{I_4}{J}\mathbf{B}\cdot(\mathbf{a}\otimes\mathbf{a})
\end{aligned}
\quad , \tag{37}
$$

where the left Cauchy-Green deformation tensor $\mathbf{B}=\mathbf{F}\mathbf{F}^{\mathrm{T}}$, $\mathbf{a}$ is the fiber direction vector in the deformed configuration. The Cauchy stress $\boldsymbol{\sigma}$ can now be found by replacing transformed tensors as shown in (37) into (34):

$$
\sigma = \frac{2}{J}\Big((W_1 + I_1W_2)\mathbf{B} - W_2\mathbf{B}^2 + W_3(I_3\mathbf{1}) + W_4I_4(\mathbf{a}\otimes\mathbf{a}) + W_5I_4(\mathbf{a}\otimes\mathbf{a}\cdot\mathbf{B} + \mathbf{B}\cdot\mathbf{a}\otimes\mathbf{a})\Big) \ . \tag{38}
$$

The symmetric fourth order material elasticity tensor $\mathbb{C}$ of the strain energy equation W can be calculated from the strain energy equation or the 2nd P-K stress as follows:

$$
\mathbb{C} = 4\frac{\partial^2 W}{\partial \mathbf{C}^2} = 2\frac{\partial \mathbf{S}}{\partial \mathbf{C}} \ . \tag{39}
$$

Calculating this derivative from (34) using the chain rule:

$$
\begin{aligned}
\frac{1}{4}\mathbb{C} = {} & \mathbf{1}\otimes\frac{\partial W_1}{\partial \mathbf{C}} + W_2\mathbf{1}\otimes\frac{\partial I_1}{\partial \mathbf{C}} + I_1\mathbf{1}\otimes\frac{\partial W_2}{\partial \mathbf{C}} - \mathbf{C}\otimes\frac{\partial W_2}{\partial \mathbf{C}} - W_2\frac{\partial \mathbf{C}}{\partial \mathbf{C}} + W_3\mathbf{C}^{-1}\otimes\frac{\partial I_3}{\partial \mathbf{C}} \\
& + I_3\mathbf{C}^{-1}\otimes\frac{\partial W_3}{\partial \mathbf{C}} + W_3I_3\frac{\partial \mathbf{C}^{-1}}{\partial \mathbf{C}} + \mathbf{a}_0\otimes\mathbf{a}_0\otimes\frac{\partial W_4}{\partial \mathbf{C}} + \frac{\partial I_5}{\partial \mathbf{C}}\otimes\frac{\partial W_5}{\partial \mathbf{C}} + W_5\frac{\partial^2 I_5}{\partial \mathbf{C}^2}
\end{aligned}
\ . \tag{40}
$$

In order to calculate the derivatives in (40) the following notation is introduced. For symmetric second order tensors **A** and **B**:

$$\begin{aligned}\left(\mathbf{A}\otimes\mathbf{B}\right)_{ijkl} &= A_{ij}B_{kl}\\ \left(\mathbf{A}\underline{\overline{\otimes}}\mathbf{B}\right)_{ijkl} &= \frac{1}{2}\left(A_{ik}B_{jl}+A_{il}B_{jk}\right)\end{aligned}. \tag{41}$$

The derivatives with respect to **C** as noted in (40) are as follows:

$$\begin{aligned}\frac{\partial\mathbf{C}}{\partial\mathbf{C}} &= \mathbf{1}\underline{\overline{\otimes}}\mathbf{1}\\ \frac{\partial\mathbf{C}^{-1}}{\partial\mathbf{C}} &= -\mathbf{C}^{-1}\underline{\overline{\otimes}}\mathbf{C}^{-1}\\ \frac{\partial^2 I_5}{\partial\mathbf{C}^2} &= \mathbf{1}\underline{\overline{\otimes}}(\mathbf{a}_0\otimes\mathbf{a}_0)+(\mathbf{a}_0\otimes\mathbf{a}_0)\underline{\overline{\otimes}}\mathbf{1}\end{aligned}, \tag{42}$$

and:

$$\begin{aligned}\frac{\partial W_\alpha}{\partial\mathbf{C}} &= \sum_{\alpha=1}^{5}\frac{\partial}{\partial\mathbf{C}}\left(\frac{\partial W}{\partial I_\alpha}\right)=\sum_{\alpha=1}^{5}\frac{\partial W_\alpha}{\partial I_\beta}\frac{\partial I_\beta}{\partial\mathbf{C}}\\ &= (W_{\alpha1}+I_1W_{\alpha2})\mathbf{1}-W_{\alpha2}\mathbf{C}+W_{\alpha3}I_3\mathbf{C}^{-1}+W_{\alpha4}(\mathbf{a}_0\otimes\mathbf{a}_0)+W_{\alpha5}(\mathbf{a}_0\otimes\mathbf{C}\cdot\mathbf{a}_0+\mathbf{a}_0\cdot\mathbf{C}\otimes\mathbf{a}_0)\end{aligned}. \tag{43}$$

Note that the derivatives $W_{\alpha\beta}$ where α and β range from 1 to 5 are the second derivatives of the strain energy with respect to the corresponding strain invariants. Replacing the derivatives in (40):

$$
\begin{aligned}
&\frac{1}{4}\mathbb{C} = (W_{11} + I_1 W_{12})(\mathbf{1}\otimes\mathbf{1}) - W_{12}(\mathbf{1}\otimes\mathbf{C}) + W_{13} I_3 (\mathbf{1}\otimes\mathbf{C}^{-1}) \\
&+W_{14}(\mathbf{1}\otimes\mathbf{a}_0\otimes\mathbf{a}_0) + W_{15}\left(\mathbf{1}\otimes(\mathbf{a}_0\otimes\mathbf{C}\cdot\mathbf{a}_0 + \mathbf{a}_0\cdot\mathbf{C}\otimes\mathbf{a}_0)\right) \\
&+W_2(\mathbf{1}\otimes\mathbf{1}) + (I_1 W_{21} + I_1^2 W_{22})(\mathbf{1}\otimes\mathbf{1}) - I_1 W_{22}(\mathbf{1}\otimes\mathbf{C}) \\
&+I_1 I_3 W_{23}(\mathbf{1}\otimes\mathbf{C}^{-1}) + I_1 W_{24}(\mathbf{1}\otimes\mathbf{a}_0\otimes\mathbf{a}_0) \\
&+I_1 W_{25}\left(\mathbf{1}\otimes(\mathbf{a}_0\otimes\mathbf{C}\cdot\mathbf{a}_0 + \mathbf{a}_0\cdot\mathbf{C}\otimes\mathbf{a}_0)\right) \\
&-(W_{21} + I_1 W_{22})(\mathbf{C}\otimes\mathbf{1}) + W_{22}(\mathbf{C}\otimes\mathbf{C}) - I_3 W_{23}(\mathbf{C}\otimes\mathbf{C}^{-1}) \\
&-W_{24}(\mathbf{C}\otimes\mathbf{a}_0\otimes\mathbf{a}_0) - W_{25}\left(\mathbf{C}\otimes(\mathbf{a}_0\otimes\mathbf{C}\cdot\mathbf{a}_0 + \mathbf{a}_0\cdot\mathbf{C}\otimes\mathbf{a}_0)\right) \\
&-W_2\left(\mathbf{1}\underline{\overline{\otimes}}\mathbf{1}\right) + I_3 W_3(\mathbf{C}^{-1}\otimes\mathbf{C}^{-1}) + (I_3 W_{31} + I_1 I_3 W_{32})(\mathbf{C}^{-1}\otimes\mathbf{1}) \\
&-I_3 W_{32}(\mathbf{C}^{-1}\otimes\mathbf{C}) + I_3^2 W_{33}(\mathbf{C}^{-1}\otimes\mathbf{C}^{-1}) + I_3 W_{34}(\mathbf{C}^{-1}\otimes\mathbf{a}_0\otimes\mathbf{a}_0) \\
&+I_3 W_{35}\left(\mathbf{C}^{-1}\otimes(\mathbf{a}_0\otimes\mathbf{C}\cdot\mathbf{a}_0 + \mathbf{a}_0\cdot\mathbf{C}\otimes\mathbf{a}_0)\right) - W_3 I_3\left(\mathbf{C}^{-1}\underline{\overline{\otimes}}\mathbf{C}^{-1}\right) \\
&+(W_{41} + I_1 W_{42})(\mathbf{a}_0\otimes\mathbf{a}_0\otimes\mathbf{1}) - W_{42}(\mathbf{a}_0\otimes\mathbf{a}_0\otimes\mathbf{C}) \\
&+I_3 W_{43}(\mathbf{a}_0\otimes\mathbf{a}_0\otimes\mathbf{C}^{-1}) + W_{44}(\mathbf{a}_0\otimes\mathbf{a}_0\otimes\mathbf{a}_0\otimes\mathbf{a}_0) \\
&+W_{45}\left(\mathbf{a}_0\otimes\mathbf{a}_0\otimes(\mathbf{a}_0\otimes\mathbf{C}\cdot\mathbf{a}_0 + \mathbf{a}_0\cdot\mathbf{C}\otimes\mathbf{a}_0)\right) \\
&+(W_{51} + I_1 W_{52})\left(\frac{\partial I_5}{\partial\mathbf{C}}\otimes\mathbf{1}\right) - W_{52}\left(\frac{\partial I_5}{\partial\mathbf{C}}\otimes\mathbf{C}\right) + I_3 W_{53}\left(\frac{\partial I_5}{\partial\mathbf{C}}\otimes\mathbf{C}^{-1}\right) \\
&+W_{54}\left(\frac{\partial I_5}{\partial\mathbf{C}}\otimes\mathbf{a}_0\otimes\mathbf{a}_0\right) + W_{55}\left(\frac{\partial I_5}{\partial\mathbf{C}}\otimes(\mathbf{a}_0\otimes\mathbf{C}\cdot\mathbf{a}_0 + \mathbf{a}_0\cdot\mathbf{C}\otimes\mathbf{a}_0)\right) \\
&+W_5\left(\mathbf{1}\underline{\overline{\otimes}}(\mathbf{a}_0\otimes\mathbf{a}_0) + (\mathbf{a}_0\otimes\mathbf{a}_0)\underline{\overline{\otimes}}\mathbf{1}\right)
\end{aligned}
\qquad (44)
$$

For ease of notation, $\frac{\partial I_5}{\partial \mathbf{C}}$ was left in its current form instead of the expanded form listed in (33). Recognizing that $W_{ab}=W_{ba}$, we can group the strain energy derivatives in (44) by their tensors:

$$
\begin{aligned}
\frac{1}{4}\mathbb{C} &= (W_{11} + 2I_1W_{12} + W_2 + I_1^2W_{22})(\mathbf{1}\otimes\mathbf{1}) - \\
&-(W_{12} + I_1W_{22})(\mathbf{1}\otimes\mathbf{C} + \mathbf{C}\otimes\mathbf{1}) \\
&+W_{22}(\mathbf{C}\otimes\mathbf{C}) - W_2\left(\mathbf{1}\underline{\overline{\otimes}}\mathbf{1}\right) \\
&+(I_3W_{13} + I_1I_3W_{23})(\mathbf{1}\otimes\mathbf{C}^{-1} + \mathbf{C}^{-1}\otimes\mathbf{1}) \\
&-I_3W_{23}(\mathbf{C}\otimes\mathbf{C}^{-1} + \mathbf{C}^{-1}\otimes\mathbf{C}) \\
&+(I_3W_3 + I_3^2W_{33})(\mathbf{C}^{-1}\otimes\mathbf{C}^{-1}) - W_3I_3\left(\mathbf{C}^{-1}\underline{\overline{\otimes}}\mathbf{C}^{-1}\right) \\
&+(W_{14} + I_1W_{24})(\mathbf{1}\otimes\mathbf{a}_0\otimes\mathbf{a}_0 + \mathbf{a}_0\otimes\mathbf{a}_0\otimes\mathbf{1}) \\
&-W_{24}(\mathbf{C}\otimes\mathbf{a}_0\otimes\mathbf{a}_0 + \mathbf{a}_0\otimes\mathbf{a}_0\otimes\mathbf{C}) \\
&+I_3W_{34}(\mathbf{C}^{-1}\otimes\mathbf{a}_0\otimes\mathbf{a}_0 + \mathbf{a}_0\otimes\mathbf{a}_0\otimes\mathbf{C}^{-1}) \\
&+(W_{15} + I_1W_{25})\left(\mathbf{1}\otimes\frac{\partial I_5}{\partial\mathbf{C}} + \frac{\partial I_5}{\partial\mathbf{C}}\otimes\mathbf{1}\right) \\
&-W_{25}\left(\mathbf{C}\otimes\frac{\partial I_5}{\partial\mathbf{C}} + \frac{\partial I_5}{\partial\mathbf{C}}\otimes\mathbf{C}\right) \\
&+I_3W_{35}\left(\mathbf{C}^{-1}\otimes\frac{\partial I_5}{\partial\mathbf{C}} + \frac{\partial I_5}{\partial\mathbf{C}}\otimes\mathbf{C}^{-1}\right) \\
&+W_{45}\left(\mathbf{a}_0\otimes\mathbf{a}_0\otimes\frac{\partial I_5}{\partial\mathbf{C}} + \frac{\partial I_5}{\partial\mathbf{C}}\otimes\mathbf{a}_0\otimes\mathbf{a}_0\right) \\
&+W_{44}(\mathbf{a}_0\otimes\mathbf{a}_0\otimes\mathbf{a}_0\otimes\mathbf{a}_0) \\
&+W_{55}\left(\frac{\partial I_5}{\partial\mathbf{C}}\otimes\frac{\partial I_5}{\partial\mathbf{C}}\right) + W_5\left(\mathbf{1}\underline{\overline{\otimes}}(\mathbf{a}_0\otimes\mathbf{a}_0) + (\mathbf{a}_0\otimes\mathbf{a}_0)\underline{\overline{\otimes}}\mathbf{1}\right)
\end{aligned}
\quad . \tag{45}
$$

The fourth order spatial elasticity tensor $\mathbb{D}$ can be found by the push forward of the material elasticity tensor $\mathbb{C}$:

$$\mathbb{D} = \varphi * \mathbb{C} \ . \tag{46}$$

In addition to the push forwards of the second order tensors listed in (37), the fourth order dyadic tensor operators listed in (41) push forward as follows:

$$
\begin{aligned}
\varphi*(\mathbf{A}\otimes\mathbf{B}) &= (\varphi*\mathbf{A})\otimes(\varphi*\mathbf{B}) \\
\varphi*(\mathbf{A}\underline{\overline{\otimes}}\mathbf{B}) &= (\varphi*\mathbf{A})\underline{\overline{\otimes}}(\varphi*\mathbf{B})
\end{aligned}
\quad . \tag{47}
$$

The final form of our spatial elasticity tensor is:

$$
\begin{aligned}
\frac{J}{4}\mathbb{D} &= (W_{11} + 2I_1W_{12} + W_2 + I_1^2W_{22})(\mathbf{B}\otimes\mathbf{B}) \\
&-(W_{12} + I_1W_{22})(\mathbf{B}\otimes\mathbf{B}^2 + \mathbf{B}^2\otimes\mathbf{B}) \\
&+W_{22}(\mathbf{B}^2\otimes\mathbf{B}^2) - W_2\mathbf{B}\underline{\overline{\otimes}}\mathbf{B} \\
&+(I_3W_{13} + I_1I_3W_{23})(\mathbf{B}\otimes\mathbf{1}+\mathbf{1}\otimes\mathbf{B}) \\
&-I_3W_{23}(\mathbf{B}^2\otimes\mathbf{1}+\mathbf{1}\otimes\mathbf{B}^2) \\
&+(I_3W_3 + I_3^2W_{33})(\mathbf{1}\otimes\mathbf{1}) - W_3I_3\left(\mathbf{1}\underline{\overline{\otimes}}\mathbf{1}\right) \\
&+(I_4W_{14} + I_1I_4W_{24})(\mathbf{B}\otimes\mathbf{a}\otimes\mathbf{a}+\mathbf{a}\otimes\mathbf{a}\otimes\mathbf{B}) \\
&-I_4W_{24}(\mathbf{B}^2\otimes\mathbf{a}\otimes\mathbf{a}+\mathbf{a}\otimes\mathbf{a}\otimes\mathbf{B}^2) \\
&+I_3I_4W_{34}(\mathbf{1}\otimes\mathbf{a}\otimes\mathbf{a}+\mathbf{a}\otimes\mathbf{a}\otimes\mathbf{1}) \\
&+(I_4W_{15} + I_1I_4W_{25})\left(\mathbf{B}\otimes(\mathbf{a}\otimes\mathbf{a}\cdot\mathbf{B}+\mathbf{B}\cdot\mathbf{a}\otimes\mathbf{a})+(\mathbf{a}\otimes\mathbf{a}\cdot\mathbf{B}+\mathbf{B}\cdot\mathbf{a}\otimes\mathbf{a})\otimes\mathbf{B}\right) \\
&-W_{25}I_4\left(\mathbf{B}^2\otimes(\mathbf{a}\otimes\mathbf{a}\cdot\mathbf{B}+\mathbf{B}\cdot\mathbf{a}\otimes\mathbf{a})+(\mathbf{a}\otimes\mathbf{a}\cdot\mathbf{B}+\mathbf{B}\cdot\mathbf{a}\otimes\mathbf{a})\otimes\mathbf{B}^2\right) \\
&+I_3I_4W_{35}\left(\mathbf{1}\otimes(\mathbf{a}\otimes\mathbf{a}\cdot\mathbf{B}+\mathbf{B}\cdot\mathbf{a}\otimes\mathbf{a})+(\mathbf{a}\otimes\mathbf{a}\cdot\mathbf{B}+\mathbf{B}\cdot\mathbf{a}\otimes\mathbf{a})\otimes\mathbf{1}\right) \\
&+W_{45}{I_4}^2\left(\mathbf{a}\otimes\mathbf{a}\otimes(\mathbf{a}\otimes\mathbf{a}\cdot\mathbf{B}+\mathbf{B}\cdot\mathbf{a}\otimes\mathbf{a})+(\mathbf{a}\otimes\mathbf{a}\cdot\mathbf{B}+\mathbf{B}\cdot\mathbf{a}\otimes\mathbf{a})\otimes\mathbf{a}\otimes\mathbf{a}\right) \\
&+{I_4}^2W_{44}(\mathbf{a}\otimes\mathbf{a}\otimes\mathbf{a}\otimes\mathbf{a}) \\
&+I_4^2W_{55}\left((\mathbf{a}\otimes\mathbf{a}\cdot\mathbf{B}+\mathbf{B}\cdot\mathbf{a}\otimes\mathbf{a})\otimes(\mathbf{a}\otimes\mathbf{a}\cdot\mathbf{B}+\mathbf{B}\cdot\mathbf{a}\otimes\mathbf{a})\right) \\
&+I_4W_5\left(\mathbf{B}\underline{\overline{\otimes}}(\mathbf{a}\otimes\mathbf{a})+(\mathbf{a}\otimes\mathbf{a})\underline{\overline{\otimes}}\mathbf{B}\right)
\end{aligned}
\quad . \qquad (48)
$$

REFERENCES

[1] Hewitt, J., Guilak, F., Glisson, R., and Vail, T. P., 2001, "Regional material properties of the human hip joint capsule ligaments," J Orthop Res, **19**(3), pp. 359-364.

[2] Lynch, H. A., Johannessen, W., Wu, J. P., Jawa, A., and Elliott, D. M., 2003, "Effect of fiber orientation and strain rate on the nonlinear uniaxial tensile material properties of tendon," J Biomech Eng, **125**(5), pp. 726-731.

[3] Screen, H. R. C., and Cheng, V. W. T., 2007, "The micro-structural strain response of tendon," J Mater Sci, **42**, pp. 8957-8965.

[4] Reese, S. P., Maas, S. A., and Weiss, J. A., 2010, "Micromechanical models of helical superstructures in ligament and tendon fibers predict large Poisson's ratios," J Biomech, **43**(7), pp. 1394-1400.

[5] Benjamin, M., and Ralphs, J. R., 1997, "Tendons and ligaments-an overview," Histol Histopathol, **12**(4), pp. 1135-1144.

[6] Lanir, Y., Salant, E. L., and Foux, A., 1988, "Physico-chemical and microstructural changes in collagen fiber bundles following stretch in-vitro," Biorheology, **25**, pp. 591-603.

[7] Hannafin, J. A., and Arnoczky, S. P., 1994, "Effect of cyclic and static tensile loading on water content and solute diffusion in canine flexor tendons: an in vitro study," J Orthop Res, **12**, pp. 350-356.

[8] Urschel, J. D., Urschel, P. G., Scott, H. T. G., and Williams, 1988, "The effect of mechanical stress on soft and hard tissue repair; a review," Brit J of Plastic Surg, **41**(2), pp. 182-186.

[9] Pioletti, D. P., Rakotomanana, L. R., Benvenuti, J. F., and Leyvraz, P. F., 1998, "Viscoelastic constitutive law in large deformations: application to human knee ligaments and tendons," J Biomech, **31**(8), pp. 753-757.

[10] Hirokawa, S., and Tsuruno, R., 2000, "Three-dimensional deformation and stress distribution in an analytical/computational model of the anterior cruciate ligament," J Biomech, **33**(9), pp. 1069-1077.

[11] Weiss, J. A., and Gardiner, J. C., 2001, "Computational modeling of ligament mechanics," Crit Rev Biomed Eng, **29**(3), pp. 303-371.

[12] Song, Y., Debski, R. E., Musahl, V., Thomas, M., and Woo, S. L., 2004, "A three-dimensional finite element model of the human anterior cruciate ligament: a computational analysis with experimental validation," J Biomech, **37**(3), pp. 383-390.

[13] Maas, S. A., Ellis, B. J., Ateshian, G. A., and Weiss, J. A., 2012, "FEBio: finite elements for biomechanics," J Biomech Eng, **134**(1), p. 011005.

[14] Frank, C. B., 2004, "Ligament structure, physiology and function," J Musculoskelet Neuronal Interact, **4**(2), pp. 199-201.

[15] Kannus, P., 2000, "Structure of the tendon connective tissue," Scand J Med Sci Sports, **10**(6), pp. 312-320.

[16] Martin, B. R., Burr, D. B., and Sharkey, N. A., 1998, *Skeletal Tissue Mechanics*, Springer-Verlag New York Inc., New York.

[17] Petersen, W., and Tillmann, B., 1999, "Structure and vascularization of the cruciate ligaments of the human knee joint," Anat Embryol (Berl), **200**(3), pp. 325-334.

[18] Quapp, K., and Weiss, J., 1998, "Material characterization of human medial collateral ligament," J Biomech Eng, **120**(6), pp. 757-763.

[19] Abramowitch, S. D., Clineff, T. D., Withrow, J. D., Papageorgiou, C. D., and Woo, S. L., 1999, "The quasilinear viscoelastic properties of the healing goat medial collateral ligament: an experimental & analytical approach," 23rd Annual Meeting of the American Society of Biomechanics, Pittsburgh, Pennsylvania.

[20] Abramowitch, S. D., Woo, S. L., Clineff, T. D., and Debski, R. E., 2004, "An evaluation of the quasi-linear viscoelastic properties of the healing medial collateral ligament in a goat model," Ann Biomed Eng, **32**(3), pp. 329-335.

[21] Bonifasi-Lista, C., Lake, S. P., Small, M. S., and Weiss, J. A., 2005, "Viscoelastic properties of the human medial collateral ligament under longitudinal, transverse and shear loading," J Orthop Res, **23**(1), pp. 67-76.

[22] Lanir, Y., Salant, E. L., and A., F., 1988, "Physico-chemical and microstructural changes in collagen fiber bundles following stretch in-vitro," Biorheology, **25**(4), pp. 591-603.

[23] Weiss, J., Bagley, A., and Blomstrong, G., 1992, "Measurement of 2-D strains in ligaments under uniaxial tension," 38th Annual Meeting, Orthopaedic Research Society, Washington, D.C., p. 662.

[24] Bonet, J., and Wood, R., 1997, *Nonlinear Continuum Mechanics For Finite Element Analysis*, Cambridge University Press, Cambridge, England.

[25] Weiss, J. A., and Maakestad, B. J., 2006, "Permeability of human medial collateral ligament in compression transverse to the collagen fiber direction," J Biomech, **39**(2), pp. 276-283.

[26] Reese, S. P., and Weiss, J. A., 2013, "Tendon fascicles exhibit a linear correlation between poisson's ratio and force during uniaxial stress relaxation," J Biomech Eng, **135**(3).

[27] Buckley, M. R., Sarver, J. J., Freedman, B. R., and Soslowsky, L. J., 2013, "The dynamics of collagen uncrimping and lateral contraction in tendon and the effect of ionic concentration," J Biomech, **46**(13), pp. 2242-2249.

[28] Lakes, R. S., and Vanderby, R., 1999, "Interrelation of creep and relaxation: a modeling approach for ligaments," J Biomech Eng, **121**(6), pp. 612-615.

[29] Provenzano, P. P., Lakes, R. S., Corr, D. T., and Vanderby, R., Jr., 2002, "Application of nonlinear viscoelastic models to describe ligament behavior," Biomech Model Mechanobiol, **1**(1), pp. 45-57.

[30] Weiss, J. A., Gardiner, J. C., and Bonifasi-Lista, C., 2002, "Ligament material behavior is nonlinear, viscoelastic and rate-independent under shear loading," J Biomech, **35**(7), pp. 943-950.

[31] Humphrey, J. D., 2002, *Cardiovascular Solid Mechanics: Cells, Tissues, and Organs*, Springer, New York.

[32] Spencer, A. J. M., 1980, *Continuum Mechanics*, Longman, London, New York.